Polymer 109 (2017) 339–348

Contents lists available at ScienceDirect

Polymer

journal homepage: www.elsevier.com/locate/polymer

Poly(alkyl methacrylate)-grafted silica nanoparticles in polyethylene nanocomposites

Mohammad M. Khani [a], Dongjin Woo [b], Edward L. Mumpower [b], Brian C. Benicewicz [a, *]

[a] Department of Chemistry and Biochemistry, University of South Carolina, Columbia, SC 29208, USA
[b] Sealed Air Corporation, 100 Rogers Bridge Road, Duncan, SC 29334, USA

ARTICLE INFO

Article history:
Received 27 September 2016
Received in revised form
12 December 2016
Accepted 15 December 2016
Available online 16 December 2016

Keywords:
Linear low density polyethylene
Poly(alkyl methacrylate)
Polymer-grafted-nanoparticles

ABSTRACT

Surface-initiated reversible addition-fragmentation chain transfer (SI-RAFT) polymerization has been widely used to synthesize various polymers grafted from nanoparticles (NPs) for incorporation into polymer nanocomposites. It is believed that these grafted polymer brushes, with a similar chemistry as the matrix polymer, can be employed to improve NP dispersion by reducing unfavorable interactions between the inorganic NPs and organic matrices. While controlled radical polymerization methods do not allow the polymerization of polyolefins, a substitute strategy is controllably attaching polyolefin-like polymers onto the NP surface. In the present work, the SI-RAFT polymerization was used to anchor poly(hexyl, lauryl, and stearyl methacrylate) on silica NPs, showing good control of the polymerizations. The long alkyl side chains can create an "olefin-like" interface and improve the compatibility of modified particles with polyolefins. Subsequently, we investigated the dispersion of these poly(alkyl methacrylate)-modified silica NPs in linear low density polyethylene (LLDPE). Poly(stearyl methacrylate)-grafted silica NPs (PSMA-g-SiO_2) demonstrated improved dispersion of particles when compared to shorter alkyl side chain methacrylates. TEM images showed that the dispersion of these particles was highly dependent upon the molecular weight and density of the grafted PSMA chains. Differential scanning calorimetry (DSC), wide-angle X-ray scattering (WAXS), small-angle X-ray scattering (SAXS), and dynamic mechanical analysis (DMA) were used to characterize these nanocomposites. SAXS showed that the inter-particle distance (distribution of particle spacings) in the semicrystalline state was broader than in the melt, suggesting that particles spacing was affected by the polyethylene crystallization particularly at lower loadings. Nanocomposites at low loadings, 0.5 wt% core content, showed significant improvement in storage modulus due to the compatible particle-matrix interface. Further increases in particle loadings, however reversed this trend likely due to the increase in soft PSMA content.

1. Introduction

It has been well accepted that the incorporation of a small volume fraction of nanoparticles into a polymer matrix can lead to a large property enhancement [1,2]. However, these enhancements depend strongly on the NPs dispersion and the nature of the nanoparticle–polymer interface [3–5]. One strategy to control the interface is to covalently attach a polymer with the same chemistry as that of the matrix onto the surface of NPs. Other variables influencing the interface are the grafting density and the chain length of the grafted polymer. Control over such variables can be used to create an attractive interface due to the better entanglement and wetting of the grafted chains and the matrix [6–9]. For example, we have shown that grafting of polystyrene chains onto the silica nanoparticles in a suitable range of chain densities and chain lengths and mixing it with polystyrene matrix can result in superior dispersion and offer improved mechanical properties [10–12].

In contrast to the case of non-crystalline polystyrene nanocomposites, dispersion of NPs in polyolefins is a greater challenge. Polyolefins are semi-crystalline polymers with phase separated amorphous and crystalline domains. As the size of the particles decreases to the nano-level and especially smaller than higher-order structures in semi-crystalline polymers, particles can

* Corresponding author.
E-mail address: benice@sc.edu (B.C. Benicewicz).

http://dx.doi.org/10.1016/j.polymer.2016.12.046
0032-3861/

interact with these crystalline structures which may lead to even more aggregation of NPs or changes in the matrix crystalline structure [13,14].

Polyethylene (PE) is one of the most important and widely used plastics due to its inertness, low cost, good processability, light weight, and good mechanical properties [15,16]. PE nanocomposites are conventionally prepared by extreme extrusion mixing of inorganic particles with the polymer in the melt which in most cases leads to large aggregates, significantly decreasing reinforcement [17]. In recent years, a variety of new methods have been proposed for improving the dispersion of particles in PE. In situ particle synthesis within the polymer matrix as well as attachment of Ziegler-Natta catalysts on nanoparticle surfaces followed by ethylene polymerization have been reported [18–21]. However, these methods have the disadvantages of complexity, possible aggregation of particles and inhomogeneous dispersion throughout the matrix. Another method which has attracted more attention is grafting a type of alkyl molecule or an end-functionalized PE onto the particle surface through chemical bonding (grafting-to method) [14,17]. This method has shown some improvements in the dispersion of particles as well as in the interactions between the modified particles and the matrix. However, this method is restricted to low graft densities and low molecular weights because of the steric hindrance imposed by the already grafted chains, while it has been well established that high graft density brushes are necessary to screen attractive van der Waals interactions between particle cores [22,23]. An alternative is the grafting-from approach in which the initiating sites are attached to the substrate surface. Polymerization is then conducted from the particle surface to prepare polymer-grafted NPs [24,25]. We have previously shown that the grafting-from strategy has advantages over the grafting-to since we can achieve a wide range of chain densities and molecular weights by performing the radical polymerization of the desired monomer on the surface of substrate [26]. While controlled radical polymerization methods do not allow the polymerization of PE, a substitute strategy could be controllably attaching polyolefin-like polymers onto the NP surface. In this work, we studied the RAFT polymerization of long side-chain methacrylates on silica NPs. These polymers were chosen because of the chemical similarity of their “olefin-like” side-chains to PE. We then investigated the dispersion and properties of the poly(-alkyl methacrylate)-modified silica NPs with different side-chain lengths, chain densities, and overall chain lengths in a linear low density polyethylene (LLDPE) matrix.

2. Experimental

2.1. Materials

LLDPE (Dowlex 2045, Mn = 34676 g/mol, PDI = 3.55) was supplied by Sealed Air Co. HPLC grade anhydrous THF was purchased from Fisher Scientific and used without further purification. Colloidal silica nanoparticles (15 nm, 30 wt % in methyl isobutyl ketone (MIBK)) were supplied by Nissan Chemicals Inc. Lauryl methacrylate (97%, Acros), stearyl methacrylate (95%, TCI America), and hexyl methacrylate (98%, TCI America) were passed through a basic alumina column to remove the inhibitor before use. Other materials utilized in the RAFT polymerization synthesis of grafted nanoparticles have been reported earlier [22].

2.2. Synthesis of CPDB-g-SiO_2 nanoparticles

In a typical experiment, a solution (20 mL) of colloidal silica particles (30 wt % in methyl isobutyl ketone) was added to a two-necked round bottom flask and diluted with 40 mL of THF. 3-Aminopropyldimethylethoxysilane (0.32 mL, 2 mmol) was added and the mixture was refluxed in a 75 °C oil bath for 5 h under nitrogen protection. The reaction was then cooled to room temperature and precipitated in a large amount of hexanes (300 mL). The particles were then recovered by centrifugation and dispersed in THF using sonication and precipitated in hexanes again. The amine-functionalized particles were then dispersed in 40 mL of THF for further reaction. Then 0.2 g, (0.4 mmol) of activated 4-cyano-4-(phenylcarbonylthioylthio)pentanoate (CPDB) was prepared as described previously [26] and added dropwise to a THF solution of the amine functionalized silica nanoparticles (40 mL, 6 g) at room temperature. After complete addition, the solution was stirred overnight. The reaction mixture was then precipitated into a large amount of hexanes (300 mL). The particles were recovered by centrifugation at 3000 rpm for 8 min. The particles were redispersed in 30 mL THF using sonication and precipitated in hexanes. This dissolution–precipitation procedure was repeated two more times until the supernatant layer after centrifugation was colorless, indicating the complete removal of ungrafted CPDB from the particles. The pink CPDB-anchored silica nanoparticles were dried under vacuum at room temperature and analyzed using UV analysis to determine the chain density using a calibration curve constructed from standard solutions of free CPDB.

2.3. Surface-initiated RAFT polymerization of alkyl methacrylate

CPDB-g-SiO_2 NPs with surface density of 41.9 μmol/g (6 g, 0.251 mmol), monomer (125.7 mmol), THF (1 L), and AIBN initiator (0.025 mmol) with a ratio between species of [monomer]:[CTA]:[initiator] = 500:1:0.1 were added to a round bottom flask. The particles were dispersed into the solution via sonication for 2 min and subsequently the mixture was purged by nitrogen for 30 min and then was placed in an oil bath set at 60 °C. The polymerization was stopped after various times (hr) by quenching in ice water. The resultant polymer grafted particles were then precipitated into a large amount of isopropanol and centrifuged at 5000 rpm for 5 min and the particles were dispersed back into THF. A small number of particles were set aside and the chains were cleaved using hydrofluoric acid and analyzed for molecular weight and PDI measurements.

2.4. Composite preparation

Various poly(alkyl methacrylate)-modified NPs solutions in THF were mixed with a 5% solution of LLDPE in toluene in appropriate quantities at 100 °C. The solution was stirred for 10 min and was cast on glass and dried in vacuum for 24 h and then annealed at 150 °C for several hours. The final film was peeled off to be used for further characterizations.

2.5. Instrumentation

The composites were embedded in epoxy and cryo-microtomed at −160 °C into 100–150 nm slices using a diamond knife. Sections were collected on a copper grid for transmission electron microscopy (TEM). The microstructures were imaged on a Hitachi H8000 TEM operating at an accelerating voltage of 200 kV. TGA characterization was operated using a TA Instruments Q5000 with a heating rate of 10 °C/min from 25 °C to 1000 °C under nitrogen flow. NMR spectra for kinetic studies were recorded on a Varian 300 spectrometer using $CDCl_3$ as a solvent. Molecular weights and dispersity ($Đ$) were measured using a Polymer Labs PL-GPC-120 gel permeation chromatograph (GPC) associated with a 515 HPLC pump, a 2410 refractive index detector, and three Styragel columns. The columns consisted of HR1, HR3 and HR4 which have

corresponding effective molecular weight ranges of 100–5000, 500–30000, and 5000–500000, respectively. The GPC used tetrahydrofuran (THF) as eluent at 30 °C and a flow rate of 1.0 mL/min with the calibration of poly(methyl methacrylate) standards obtained from Polymer Laboratories. Differential scanning calorimetry (DSC) was performed using a TA Instruments DSC Q-2000 with steady heating and cooling rates of 10 °C/min and nitrogen flow rate of 20 mL/min. Dynamic mechanical analysis tests were performed using a TA Instruments RSAIII dynamic mechanical analyzer (DMA). The tests were run on 0.2 mm thick films from −140 to 100 °C, using a heating rate of 3 °C min^{-1}. They were performed in tensile mode with strain rate of 0.1% and at frequency of 1 Hz. Small-angle X-ray scattering (SAXS) experiments were conducted using a SAXS LAB Ganesha at the South Carolina SAXS Collaborative of the University of South Carolina. A Xenocs GeniX3D microfocus source was used with a copper target to generate a monochromic beam with a 0.154 nm wavelength. The instrument was calibrated using a silver behenate reference with the first order scattering vector $q^* = 1.076\ nm^{-1}$, where $q = 4\pi\lambda^{-1}\sin\theta$ with a total scattering angle of 2θ. Each data set was acquired for about 30 min with an incident X-ray flux of ~1.5 M photons/s. Samples were first analyzed at room temperature and then heated to 150 °C for 1 h and analyzed in the melt in order to compare the dispersion of particles.

3. Results and discussion

3.1. Surface initiated RAFT polymerization of alkyl methacrylate

Scheme 1 shows three different polymers studied in this work: Poly(hexyl methacrylate) (PHMA), poly(lauryl methacrylate) (PLMA), and poly(stearyl methacrylate) (PSMA). PLMA and PSMA are semicrystaline polymers since their alkyl side chains crystallize in spite of an amorphous backbone [27].

Using the grafting-from approach, we have previously demonstrated the synthesis of polymer-grafted particles using the RAFT polymerization technique from surface-anchored chain transfer agents, which in this work were used to prepare poly(alkyl methacrylate)-g-silica NPs (Scheme 2) [26]. In this process, a mercaptothiazoline activated-CPDB (4-cyano-4-(phenylcarbonylthioylthio)pentanoate) chain transfer agent was anchored onto the surface of silica nanoparticles functionalized with amine groups. This approach has been used to prepare CPDB-grafted silica nanoparticles (CPDB-g-SiO_2) with graft densities varying from 0.01 to 0.68 RAFT agents/nm^2 by controlling the ratio of silica nanoparticles to 3-aminopropyldimethylethoxysilane [26,28].

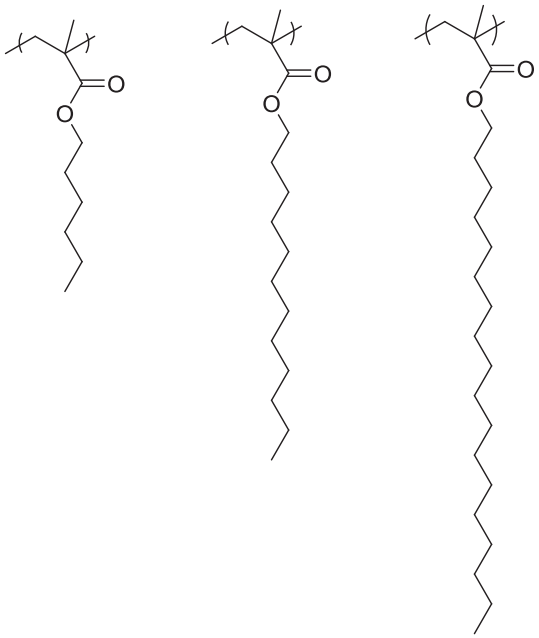

Scheme 1. Chemical structures of poly(hexyl, lauryl, and stearyl methacrylates).

We have previously reported the synthesis and kinetic studies of the surface-initiated RAFT polymerization of HMA [29]. Here we studied the RAFT polymerization of SMA and LMA in solution and on the surface of nanoparticles. SI-RAFT polymerization of stearyl methacrylate was carried out from the surface of CPDB-g-SiO_2 to give poly(stearyl methacrylate) brush-anchored silica nanoparticles (PSMA-g-SiO_2). Azobisisobutyronitrile was used as the initiator and a 10:1 [CPDB]/[AIBN] ratio utilized for all polymerizations. Low AIBN concentrations minimized the amount of free polymer and still maintained a moderate polymerization rate [24]. The weight ratio of THF/SMA was kept high (~6) for all SMA polymerizations since high concentrations of hydrophobic SMA caused silica particles to aggregate. Therefore, particles were diluted down in THF prior to addition of monomer. The polymerization reaction was carried out at 60 °C for a desired time and then precipitated in methanol. PSMA chains were etched from the silica nanoparticles by hydrofluoric acid and were analyzed by GPC analysis. The GPC traces of the cleaved PSMA and PLMA are shown in Figs. S1 and S2 respectively.

The kinetic study of SI-RAFT polymerization of SMA on nanoparticles (coated CPDB density: 0.16 agents/nm^2) was followed over 19 h to demonstrate the living character of the RAFT process. Fig. 1a shows the pseudo-first-order rate plot for this polymerization. The ratio between the species of [SMA]/[CPDB]/[AIBN] was 1000:1:0.1 in THF with a monomer concentration of 25% wt/vol. Conversion of monomer was determined by ^1H NMR by comparing the vinyl hydrogens of the monomer with those of trioxane. A linear relationship between $\ln([M_0]/[M_t])$ (where M_0 is the initial monomer concentration and M_t is the monomer concentration at time t) and polymerization time was observed after an induction time of 3 h, which implies a constant radical concentration. The Mn determined by GPC (calibrated with PMMA standards) increased nearly linearly with monomer conversion for molecular weight up to approximately 100 kg/mol. (Fig. 1b). The higher experimental molecular weights (compared to the theoretical) are likely due to the use of PMMA standards in GPC analysis. The same trend was observed for the kinetic studies of the solution RAFT polymerization of SMA and LMA (Figs. S3 and S4). Demetriou et al. [30] have reported similar observations for the RAFT polymerization of LMA in benzene and related this difference to the partial CTA deactivation. However, we believe this difference arises from the relative molecular weights obtained from a GPC calibrated with PMMA standards.

The dispersity for the SI-RAFT polymerization of SMA ($Đ$ ~ 1.4) was larger at higher molecular weights compared to solution polymerization of SMA ($Đ$ ~ 1.2) (Fig. S3). This could be attributed to either the dilute polymerization media (solvent to monomer ratio was ~6) which would increase the dispersity by limiting the access of monomer to the growing chain, or that the bulky immobilized PSMA chains on the particle hinder access of the growing radicals to the monomers.

The kinetic study of the SI-RAFT polymerization of LMA is shown in Fig. 2. It was performed by the same method and conditions as for SMA. However, the polymerization of LMA proceeded to higher monomer conversions and higher molecular weights. This result may be attributed to the smaller size of LMA monomer compared to SMA, which then allows for easier access of monomers

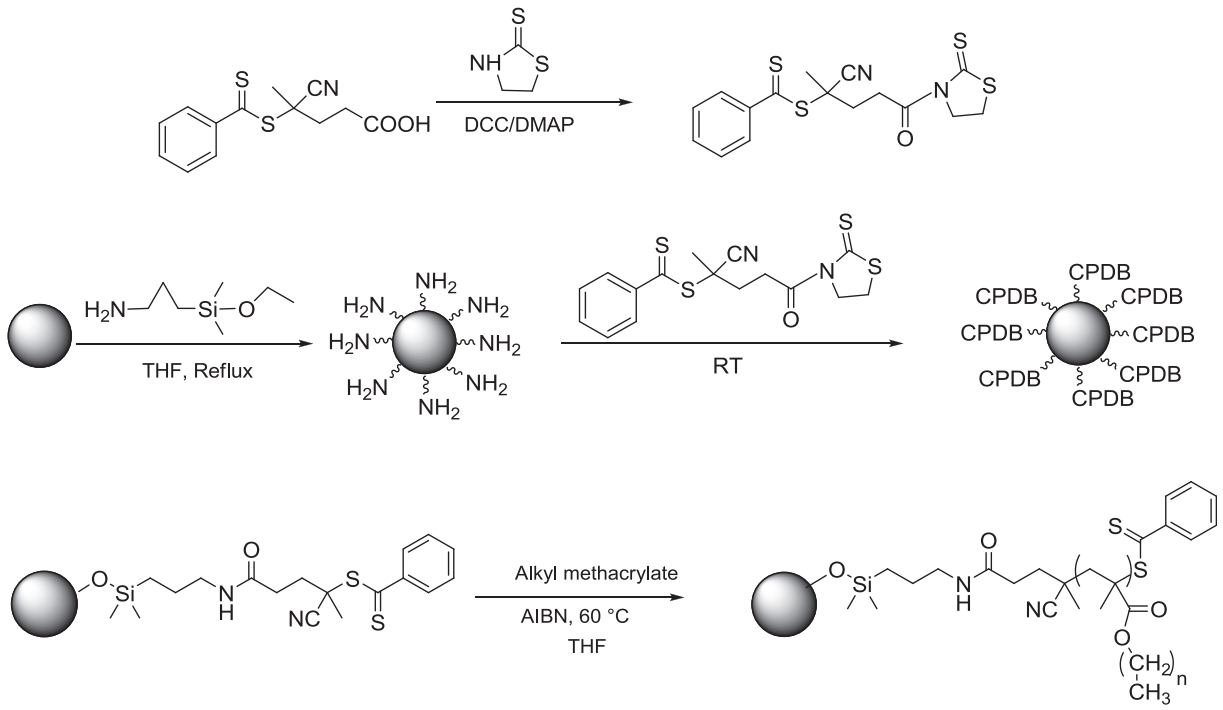

Scheme 2. Modification of silica nanoparticles by poly(alkyl methacrylates) using the RAFT technique.

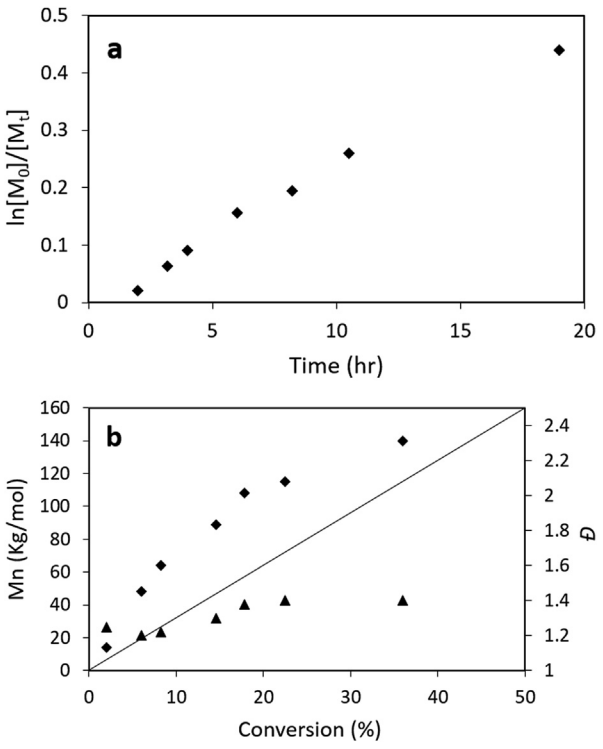

Fig. 1. (a) Kinetic plot and (b) dependence of the GPC molecular weight (diamond), theoretical molecular weight (solid line), and dispersity (triangle) on the conversion for the surface-initiated RAFT polymerization of stearyl methacrylate on modified nanoparticles with CPDB density: 0.16 agents/nm^2 ([SMA]/[CPDB]/[AIBN] = 1000:1:0.1).

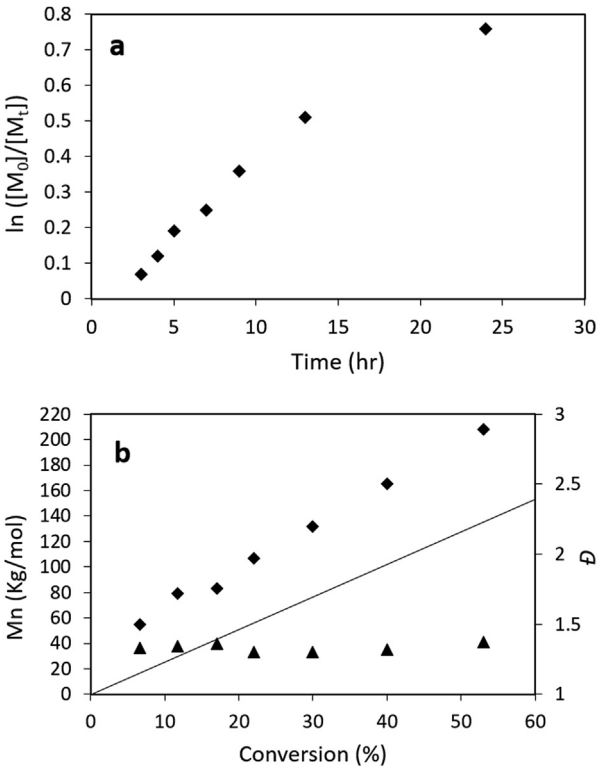

Fig. 2. (a) Kinetic plot and (b) dependence of the GPC molecular weight (diamond), theoretical molecular weight (solid line), and dispersity (triangle) on the conversion for the surface-initiated RAFT polymerization of lauryl methacrylate on modified nanoparticles with CPDB density: 0.16 agents/nm^2 ([LMA]/[CPDB]/[AIBN] = 1000:1:0.1).

to the growing radicals.

The surface initiated RAFT polymerization method described above was then used to prepare several different polymer-grafted particles, some of which are summarized in Table 1. PHMA, PLMA, and PSMA grafted NPs were synthesized at a constant chain

Table 1
Various poly(alkyl methacrylate)-g-SiO_2 NPs synthesized using RAFT polymerization.

Number	Polymer	Graft density, chains/nm^2	MW, Kg/mol
NP-1	PHMA	0.16	70
NP-2	PLMA	0.16	165
NP-3	PSMA	0.16	115
NP-4	PSMA	0.06	132
NP-5	PSMA	0.03	121
NP-6	PSMA	0.16	10
NP-7	PSMA	0.16	40
NP-8	PSMA	0.33	86

density of 0.16 ch/nm^2 with molecular weights of 70, 165, and 115 kg/mol, respectively. Then, PSMA-g-SiO_2 with various chain densities and molecular weights were also synthesized (see Table 1).

3.2. LLDPE nanocomposites filled with various poly(alkyl methacrylate)-grafted nanoparticles

The main goal of this study was to investigate the compatibility of various poly(alkyl methacrylate) grafted silica NPs with a polyolefin such as LLDPE. During the preparation of this paper, Sanchez et al. [31] reported on the preparation of low density polyethylene nanocomposites filled with poly(lauryl methacrylate) grafted Al_2O_3 nanoparticles. However, they did not fully investigate the role of the molecular graft variables on the dispersion of nanoparticles in the matrix. Moreover, this work reports significant differences between lauryl methacrylate and the longer stearyl methacrylate and their compatibility with polyethylene matrices.

To study the effect of different chemistries on the dispersion and the properties of LLDPE nanocomposites, PHMA, PLMA, and PSMA-grafted NPs (NP-1, NP-2, and NP-3 from Table 1) were prepared and studied. Samples were prepared at 4 wt% silica core loading which were determined by Thermogravimetric Analysis (TGA). Fig. 3 shows the TGA measurements for PSMA-g-SiO_2 (NP-3) and NP-3 mixed with LLDPE at 4 wt% silica core loading.

The dispersion of the grafted silica NPs was examined using Transmission Electron Microscopy (TEM). Fig. 4 shows a representative comparison of dispersion states for nanocomposites filled with bare silica, PHMA, PLMA, and PSMA-grafted nanoparticles. Nanocomposites filled with bare silica (Fig. 4a) showed a compact aggregation of particles due to the incompatibility and poor interface between silica and PE. PHMA-g-SiO_2 also showed particle aggregates (Fig. 4b). Although the particles were grafted with PHMA,

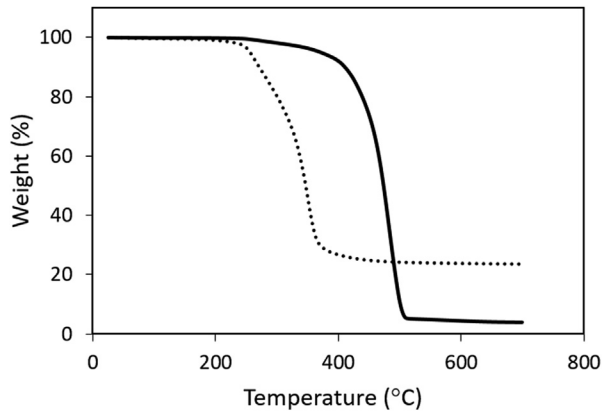

Fig. 3. TGA curves for the NP-3 nanoparticles (dashed line) and 4 wt% NP-3/LLDPE composite (solid line).

micrometer size agglomerates still formed due to the incompatibility between the PHMA brush and PE matrix. We suggest that the hexyl side chain in PHMA does not make the PHMA sufficiently "olefin-like" and the mixing is thus enthalpically unfavorable. PLMA-g-SiO_2, with a dodecyl pendent group, is more olefin-like compared to PHMA and showed some level of compatibility with PE (Fig. 4c). The TEM images of PLMA-g-SiO_2 showed less firmly packed agglomerates than the bare silica and PHMA-g-SiO_2 filled nanocomposites. The compact agglomerated structures observed previously were not observed, instead replaced by swollen self-associated structures (intermediate morphology). Fig. 4d shows the TEM image for nanocomposites filled with PSMA-g-SiO_2 nanoparticles with randomly distributed particles. PSMA, with 18 carbon side chains, is believed to be sufficiently olefin-like to show a good level of compatibility with PE. Since PSMA-g-SiO_2 particles showed better compatibility with the PE matrix, these particles were the focus for further studies.

3.3. Effect of grafting chain densities

In order to investigate the role of polymer chain grafting density on the dispersion of PSMA-g-SiO_2 NPs in a PE matrix, PSMA-g-SiO_2 NPs with chain densities of 0.03, 0.06, 0.16 and 0.33 ch/nm^2 with molecular weights of 121, 132, 115, and 86 kg/mol, respectively, were synthesized. Fig. 5 shows the TEM micrographs of the nanocomposites attributed to these samples. It is evident that as the chain density increased, the dispersion of the particles improved. A chain density of 0.03 ch/nm^2 corresponds to about 20 chains per particle which appears to be insufficient to screen the core-core interactions between silica particles leading to large aggregated structures. The 0.06 ch/nm^2 particles also appeared insufficient to alleviate the core-core interactions between silica particles. However, the sizes of the agglomerates were smaller than nanocomposites prepared with 0.03 ch/nm^2 particles. Particles with densities of 0.16 and 0.33 ch/nm^2 showed much improved dispersions of particles. The density of 0.16 ch/nm^2 corresponds to about 100 polymer chains per particle and is believed to be enough to moderate the core-core interactions. It is worth mentioning that the molecular weights of the PSMA brushes were chosen to ensure that the chain segments at the outer portions of the nanoparticles would be in the semi-dilute brush conformations.

3.4. Effect of grafted polymer chain length

In order to investigate the role of grafted PSMA chain length on the nanoparticles dispersion, PSMA-g-SiO_2 NPs at the same chain density of 0.16 ch/nm^2 with different molecular weights of 10, 40, and 115 kg/mol were prepared and used to fabricate LLDPE nanocomposites (Table 1). Fig. 6 shows a comparison of TEM micrographs of these nanocomposites. The dispersion of nanoparticles is evidently improved with the increase in the molecular weight of the grafted PSMA. Particles with 10 kg/mol grafted PSMA formed large agglomerates, despite the compatibility of the grafted chains and matrix chains discussed earlier. Although the particles were grafted with PSMA chains to screen the core-core attractions, particles still aggregated because of the poor entanglement between the short grafted PSMA and long LLDPE chains (matrix cannot wet the polymer-grafted particles) [6–9,22]. Increasing the molecular weight of the PSMA brush to 40 kg/mol improved the entanglement but not sufficient to fully disperse the nanoparticles. When the grafted chain length finally increased to 115 kg/mol, favorably interaction and entangle with the matrix chains led to spatially dispersed particles.

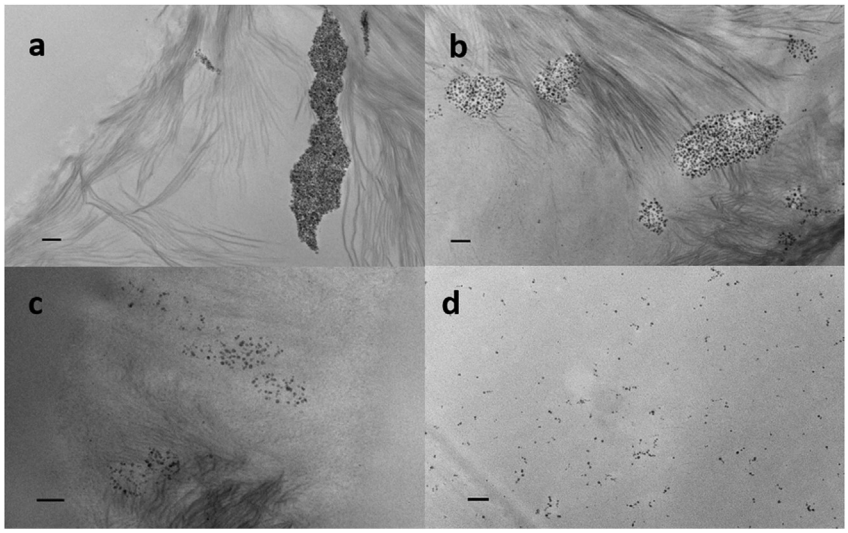

Fig. 4. TEM micrographs of LLDPE nanocomposites filled with 4% loading of a) bare silica, b) PHMA-g-silica (NP-1), c) PLMA-g-silica (NP-2), and d) PSMA-g-silica (NP-3) at a fixed chain density of 0.16 ch/nm^2 (scale bars are 200 nm).

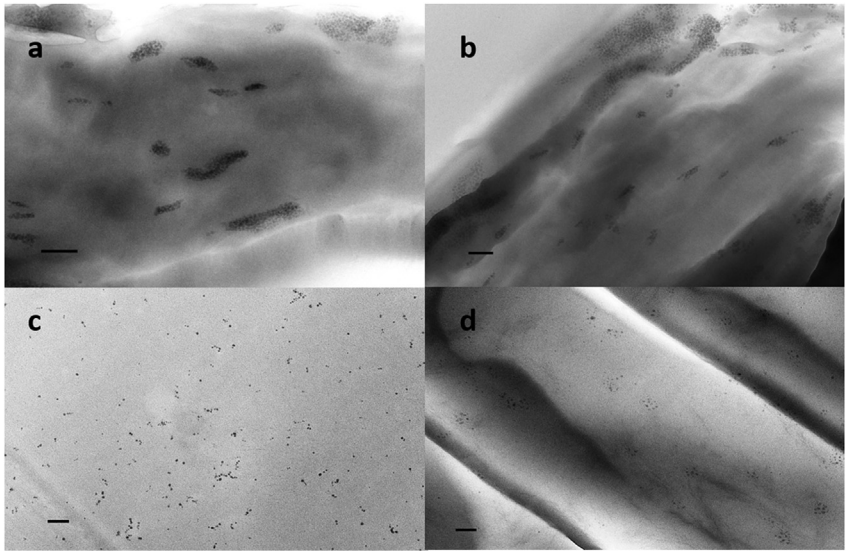

Fig. 5. TEM micrographs of LLDPE nanocomposites filled with approximately 4% silica loading of PSMA-g-silica NPs with chain densities of a) 0.03 (NP-5), b) 0.06 (NP-4), c) 0.16 (NP-3), and 0.33 ch/nm^2 (NP-8). (Scale bars are 200 nm).

3.5. Characterization of PSMA-g-SiO_2 filled LLDPE nanocomposites

The composite with NP-3 (highly dispersed sample) was used for initial screening studies to probe the interactions between the PSMA-g-SiO_2 particles and LLDPE. Composites with 10, 20, 30, 40, and 60 wt% PSMA-g-SiO_2 nanoparticles were prepared which contained 2, 4, 6, 8, and 12 wt% core silica, respectively (Table 2). Samples were solution cast on glass and after solvent evaporation, annealed for 24 h. DSC was used to study the thermal properties of the composites (Fig. 7). The temperature was increased at a rate of 10 °C/min from −50 to 150 °C and then cooled at 10 °C/min to −50 °C. This was repeated two times per specimen. Data from the first cycle was not considered in order to eliminate thermal history effects. The cyclic heating-cooling DSC curves for LLDPE filled with 20% PSMA-g-SiO_2 (NP-3) are illustrated in Fig. S5.

The unfilled LLDPE showed a peak at 124 °C for the melting transition with a shoulder at ~113 °C which was attributed to the composition distribution of the side chains in the LLDPE. This peak did not move with addition of up to 60 wt% particles. The crystallization peak for the unfilled LLDPE was at 110.1 °C. This peak also did not seem to be greatly affected by the incorporation of particles. Composites containing PSMA-g-SiO_2 showed a melting transition at 30 °C attributed to the side-chain crystallization of PSMA which increased with increasing particles loading. It is worth mentioning that the melting transition for the pure PSMA-g-SiO_2 was 33 °C which is higher than that of the related composite. The decrease for the melting point could be due to the perturbation of the molecular ordering of PSMA in the composite [32].

Wide angle x-ray scattering (WAXS) patterns of neat LLDPE and 20% filled composite shown in Fig. 8 show two main peaks at 21.5 and 23.6° (2θ) which correspond to the (110) and (200) planes of PE [33]. The WAXS pattern of the nanocomposite shows no measurable changes in the crystalline lattice structure of the PE matrix, which suggests that the crystallinity of the LLDPE matrix is not

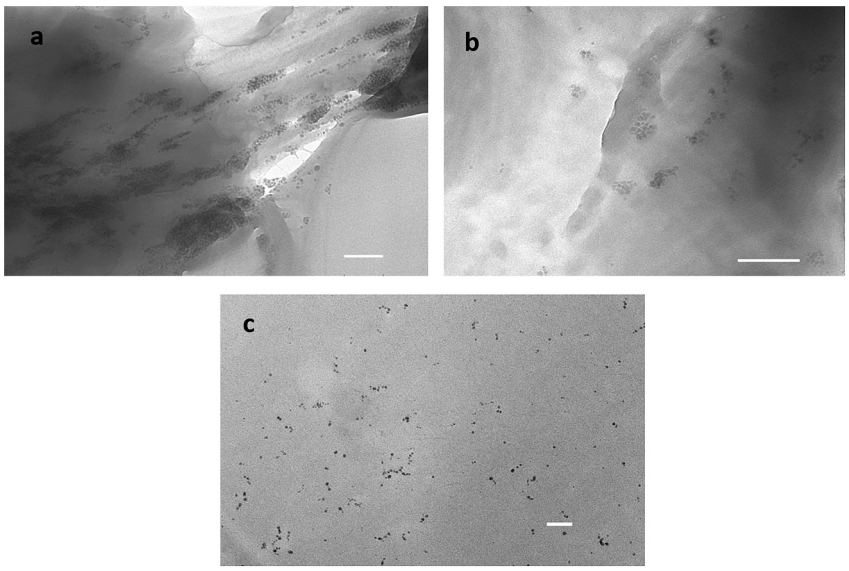

Fig. 6. TEM micrographs of LLDPE nanocomposites filled with approximately 4% silica loading of PSMA-g-silica NPs with different grafted molecular weights of a) 10 (NP-6), b) 60 (NP-7), and c) 115 kg/mol (NP-3), at a set chain density of 0.16 ch/nm^2 (Scale bars are 200 nm).

Table 2
Thermal and crystalline properties of LLDPE composites.

LLDPE/Fillers	Filler loading (wt%)[a]	T_m (°C)	T_c (°C)
LLDPE	0	123.9	110.1
LLDPE/NP-3	10	123.9	109.5
LLDPE/NP-3	20	124.5	109.2
LLDPE/NP-3	30	123.9	108.6
LLDPE/NP-3	40	124.8	108.0
LLDPE/NP-3	60	123.5	107.1

[a] The weight percent is based on the total PSMA-g-SiO_2 (nanocomposite with 20% filler contains 4% silica and 16% grafted PSMA).

affected by the particles [34].

The results from the SAXS of the 20, 40, and 60% PSMA-g-SiO_2 (NP-3) filled nanocomposites at solid state (room temperature) and melt state (140 °C) are shown in Fig. 9a and b, respectively. The scattering peak originates from the contrast between the silica particle and the polymeric matrix (~80% increase in electron density for silica over crystalline PE) which is completely different from the primary scattering contrast between the crystalline and amorphous phase (Fig. S6). The effective surface-to-surface distance between the particles, h_{eff} was determined using

$$h_{eff} = \frac{2\pi}{q_m} - d_{eff}$$

where q_m is the first-order scattering maximum and d_{eff} is the effective particle diameter which is approximately 14 nm. Using this formula h_{eff} was calculated to be 24, 19, and 17 nm for 20, 40, and 60% filler loadings, respectively, in both the melt and solid state. Therefore, mean particle spacing remained unchanged when the sample was cooled from the melt to below the crystallization temperature (T_c). However, the x-ray peaks broadened in the crystalline state (Fig. 9a). This has been quantified from the half-width-at half-maximum (Δq) on the high-q side of the peaks ($\Delta q = 0.05$, 0.04, and 0.04 nm^{-1} for 20, 40, and 60% loadings above T_m, respectively, and $\Delta q = 0.09$, 0.06, and 0.06 nm^{-1} for 20, 40, and 60% loadings below T_c, respectively). This means that the distribution of particle separation is broadened in the semicrystalline polymer. It is clear that the broadening is much more significant for the 20% filled sample compared to samples with higher particle loadings. This phenomenon has been observed in our previous work on polyethylene oxide composites filled with PMMA-g-SiO_2

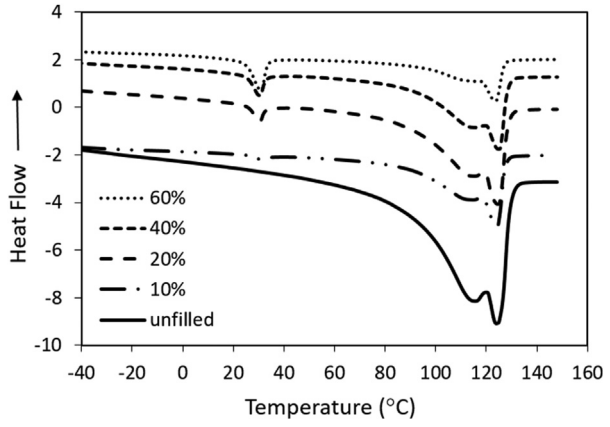

Fig. 7. DSC curves of different LLDPE systems filled with PSMA-g-SiO_2 with 0.16 ch/nm^2 density and 115 kg/mol molecular weight. Percent loading is based on total weight of filler.

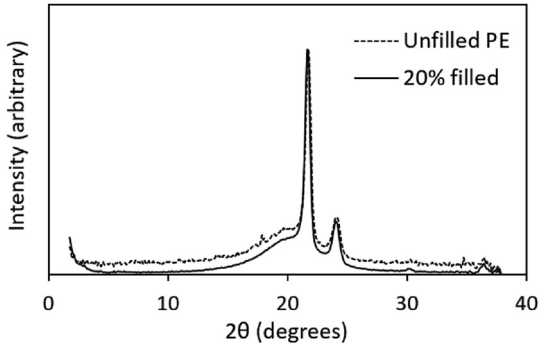

Fig. 8. WAXS results showing negligible changes in the patern for the pure LLDPE and LLDPE filled with 20% NP-3.

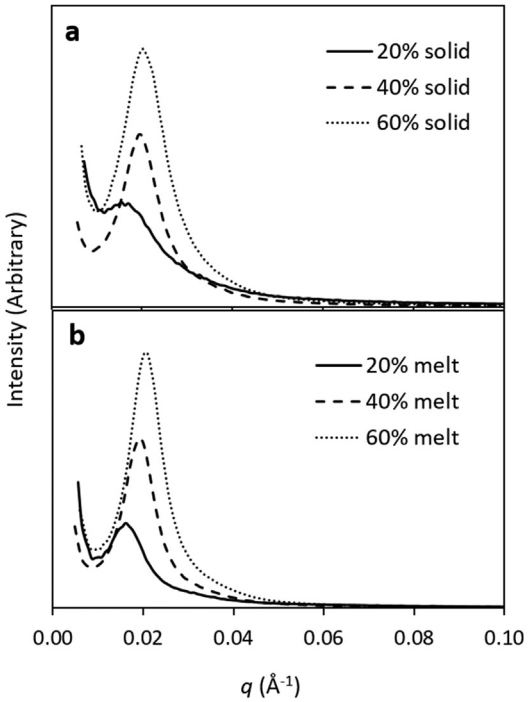

Fig. 9. SAXS results of the 20, 40, and 60% (NP-3) loading nanocomposite as a function of scattering vector, *q*, at solid state (room temperature) and melt state (140 °C). Note that the scattering peak originated from the contrast between the silica particle and the polymeric matrix (not the scattering between the crystal and amorphous phase).

NPs that showed samples with particle loadings below 20% did not contribute to the crystalline structure of the matrix and the particles are forced away from the crystalline sites [34]. This was further investigated by SAXS analysis of two 20% loading nanocomposites at room temperature. Both samples were cooled after a 24 h thermal annealing period, one quenched in liquid nitrogen and the other cooled at a rate of 0.5 °C/min (Fig. 10). The slow cooled sample showed a broader peak compared to the fast cooled sample, which indicates a broader distribution of particle separation for the slow cooled sample. This result suggests that when the composite was cooled fast, particles did not have time to move away from the crystallizing fronts and were trapped, resulting in a narrower particle separation. Therefore, we conclude from these differences especially at lower particle loadings, the growing polyethylene crystallites push some of the particles out of the way, resulting in a broader distribution of particle spacing in the solid state. TEM imaging over a range of particle loadings did not present obvious differences in dispersion, but showed that particles were generally well-dispersed within the PE matrix. Fig. 11 illustrates the TEM results for the 60% filled composite which shows a good state of dispersion even at such high loading.

Film samples (0.2 mm) of neat LLDPE, nanocomposites containing 2.5% and 12% PSMA-g-SiO_2 (NP-3), and a control sample containing 0.5% silica and 2% of free PSMA were prepared and analyzed by dynamic mechanical analysis (DMA) in the temperature range of−140−100 °C. Note that a 2.5% PSMA-g-SiO_2 composite contains 0.5% of core silica and approximately 2% of grafted PSMA. Both storage (Fig. 12) and loss moduli (Fig. S7) of all composites were increased compared to the neat LLDPE films and the increase was more significant at lower temperatures. The increases of the storage modulus at −100 °C for 2.5% control, 2.5%-NP-3, and 12%- NP-3 were found to be 15%, 87%, and 62% respectively while these increases at 25 °C for 2.5% control, 2.5%-NP-3, and 12%-NP-3, were found to be 18%, 52%, and 38%, respectively. Therefore, the composite containing 0.5% bare silica +2% free PSMA showed the smallest increase in modulus. A similar increase was observed in the case of addition of 0.5% bare silica and is consistent with previous reports for polyethylene composites [31,35,36]. These results support that a composite containing 2.5% of well-dispersed PSMA-g-silica has a greater interfacial adhesion between the particles and the matrix due to the compatibility of PSMA brushes and the polyethylene matrix which causes a better load transfer at the particle-matrix interface. The further increase of PSMA-g-SiO_2 loading to 12% did not further increase the storage modulus. This trend has been previously seen in other cases of polyethylene composites, i.e., that by increasing the nanoparticles concentration, the mechanical reinforcement becomes smaller [31,35]. This phenomenon was attributed to the possible aggregation of particles at loadings above 1%. However, we know that PSMA-g-SiO_2 particles (NP-3) were well-dispersed in LLDPE even at higher loadings, therefore other reasons could be involved in our work. A 12% PSMA-g-SiO_2 composite contains approximately 2.5% core silica and 9.5% of grafted PSMA chains. Since PSMA has much lower modulus compared to polyethylene, we believe that further increases in concentration of PSMA on the grafted particle negates the effect of the dispersed silica particles on the modulus especially at higher temperatures (melting point of PSMA is ~33 °C). Therefore, maintaining a low concentration of particles is necessary for achieving higher mechanical reinforcement. While these data confirm the compatibility of PSMA-g-SiO_2 with polyethylene, more detailed studies are needed to investigate the effect of these particles on other properties of polyethylene composites which will be

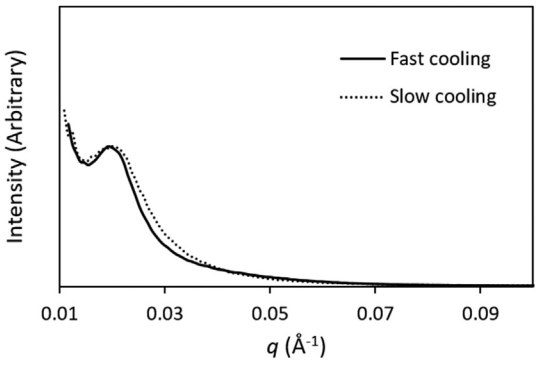

Fig. 10. SAXS results of the 20% loading nanocomposite as a function of scattering vector, q, at room temperature cooled from two annealed samples, one quenched in liquid nitrogen and the other one slowly cooled down with a rate of 0.5°/min.

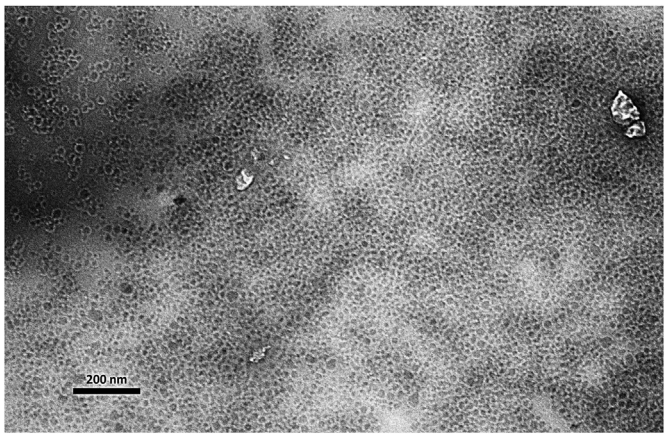

Fig. 11. TEM results for LLDPE nanocomposite filled with 60% NP-3.

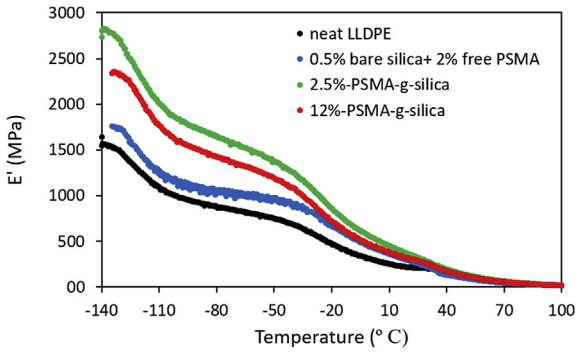

Fig. 12. Storage modulus of the LLDPE nanocomposites measured by dynamic mechanical analysis.

the focus of our research for the future.

4. Conclusions

We have demonstrated a method for the preparation of poly(-alkyl methacrylate)-grafted silica nanoparticles using surface-initiated RAFT polymerization. Composites of LLDPE filled with PHMA, PLMA, and PSMA-g-SiO_2 NPs were prepared and examined by TEM to test the effects of side chain length on the dispersibility. PSMA-g-SiO_2 showed the highest state of dispersion among the three modified particles. It was suggested that the 18 carbon long alkyl side chains make the PSMA more "olefin-like" and are responsible for the compatibility of PSMA-g-SiO_2 with polyethylene due to the molecular similarity. The graft density of PSMA chains was also shown to be crucial in the dispersion of particles throughout the matrix. Particles with lower grafting densities agglomerated where the higher densities showed improved dispersions. The agglomeration of lower graft density particles was due to the core-core interaction of silica particles. The effect of chain molecular weight was also studied and showed that low molecular weight PSMA grafted particles agglomerated and as the molecular weight increased the state of dispersion improved which was ascribed to the enhanced entanglement of high molecular weight brushes with the LLDPE matrix. DSC and WAXS revealed that PSMA-g-SiO_2 particles did not greatly affect the thermal and crystalline properties of LLDPE. SAXS studies showed the particle spacing distribution broadened when cooling the samples slowly from the melt to the crystalline state. For the nanocomposites with nanoparticle loadings especially below 20 wt%, it is likely that some of the nanoparticles were pushed out of the way of the growing crystallites, resulting in a broadening of the particle distribution. Storage and loss modulus of the samples were analyzed by DMA and showed improvement by the addition of PSMA-g-SiO_2 NPs. The storage modulus of the polyethylene improved by addition of only 2.5% PSMA-g-SiO_2 (NP-3) and this improvement was found to be more significant at lower temperatures (up to 90%). The detailed investigation of the effect of these compatible particles on the properties of polyethylene is an interesting issue that we shall probe in future work.

Acknowledgements

The authors thank Prof. Sanat Kumar and Dan Zhao (Columbia University) for useful discussions and Zack Marsh and Amrita Sarkar (University of South Carolina) for the help with the SAXS measurements and interpretation. M.M.K and B.C.B would like to acknowledge Sealed Air Corp. for their support of this work. The SAXS measurements were done at the South Carolina SAXS Collaborative, supported by the NSF Major Research Instrumentation program (DMR-1428620).

Appendix A. Supplementary data

GPC analyses of the cleaved PSMA and PLMA from the grafted particles, kinetic plots of the solution RAFT polymerizations of SMA and LMA, cyclic heating-cooling DSC curves for LLDPE filled with 20 wt% PSMA-g-SiO_2 (NP-3), Lorentz-corrected SAXS of neat PE, and the loss modulus data.

Supplementary data related to this article can be found at http://dx.doi.org/10.1016/j.polymer.2016.12.046.

References

[1] R.A. Vaia, J.F. Maguire, Polymer nanocomposites with prescribed morphology: going beyond nanoparticle-filled polymers, Chem. Mater 19 (2007) 2736–2751, http://dx.doi.org/10.1021/cm062693+.
[2] H. Zou, S. Wu, J. Shen, Polymer/silica nanocomposites: preparation, characterization, properties, and applications, Chem. Rev. 108 (2008) 3893–3957, http://dx.doi.org/10.1021/cr068035q.
[3] M.E. Mackay, A. Tuteja, P.M. Duxbury, C.J. Hawker, B. Van Horn, Z. Guan, G. Chen, R.S. Krishnan, General strategies for nanoparticle dispersion, Science 311 (2006) 1740–1743, http://dx.doi.org/10.1126/science.1122225.
[4] L.S. Schadler, S.K. Kumar, B.C. Benicewicz, S.L. Lewis, S.E. Harton, Designed interfaces in polymer nanocomposites: a fundamental viewpoint, MRS Bull. 32 (2007) 335–340, http://dx.doi.org/10.1557/mrs2007.232.
[5] S.K. Kumar, R. Krishnamoorti, Nanocomposites: structure, phase behavior, and properties, Annu. Rev. Chem. Biomol. Eng. 1 (2010) 37–58, http://dx.doi.org/10.1146/annurev-chembioeng-073009-100856.
[6] P.F. Green, The structure of chain end-grafted nanoparticle/homopolymer nanocomposites, Soft Matter 7 (2011) 7914, http://dx.doi.org/10.1039/c1sm05076a.
[7] S. Ojha, A. Dang, C.M. Hui, C. Mahoney, K. Matyjaszewski, M.R. Bockstaller, Strategies for the synthesis of thermoplastic polymer nanocomposite materials with high inorganic filling fraction, Langmuir 29 (2013) 8989–8996, http://dx.doi.org/10.1021/la401522v.
[8] A. Bansal, H. Yang, C. Li, B.C. Benicewicz, S.K. Kumar, L.S. Schadler, Controlling the thermomechanical properties of polymer nanocomposites by tailoring the polymer–particle interface, J. Polym. Sci. Part B Polym. Phys. 44 (2006) 2944–2950, http://dx.doi.org/10.1002/polb.20926.
[9] L. Meli, A. Arceo, P.F. Green, Control of the entropic interactions and phase behavior of athermal nanoparticle/homopolymer thin film mixtures, Soft Matter 5 (2009) 533–537, http://dx.doi.org/10.1039/b814714k.
[10] P. Akcora, S.K. Kumar, J. Moll, S. Lewis, L.S. Schadler, Y. Li, B.C. Benicewicz, A. Sandy, S. Narayanan, J. Ilavsky, P. Thiyagarajan, R.H. Colby, J.F. Douglas, "Gel-like" mechanical reinforcement in polymer nanocomposite melts, Macromolecules 43 (2010) 1003–1010, http://dx.doi.org/10.1021/ma902072d.
[11] A.C. Balazs, T. Emrick, T.P. Russell, Nanoparticle polymer composites: where two small worlds meet, Science 314 (2006) 1107–1110, http://dx.doi.org/10.1126/science.1130557.
[12] P. Akcora, H. Liu, S.K. Kumar, J. Moll, Y. Li, B.C. Benicewicz, L.S. Schadler, D. Acehan, A.Z. Panagiotopoulos, V. Pryamitsyn, V. Ganesan, J. Ilavsky, P. Thiyagarajan, R.H. Colby, J.F. Douglas, Anisotropic self-assembly of spherical polymer-grafted nanoparticles, Nat. Mater 8 (2009) 354–359, http://dx.doi.org/10.1038/nmat2404.
[13] T. Taniike, M. Toyonaga, M. Terano, Polypropylene-grafted nanoparticles as a promising strategy for boosting physical properties of polypropylene-based nanocomposites, Polym. Guildf. 55 (2014) 1012–1019, http://dx.doi.org/10.1016/j.polymer.2014.01.016.
[14] M. Bieligmeyer, S.M. Taheri, I. German, C. Boisson, C. Probst, W. Milius, V. Altstädt, J. Breu, H.-W. Schmidt, F. D'Agosto, S. Förster, Completely miscible polyethylene nanocomposites, J. Am. Chem. Soc. 134 (2012) 18157–18160, http://dx.doi.org/10.1021/ja307297c.
[15] A. Dorigato, A. Pegoretti, (Re)processing effects on linear low-density polyethylene/silica nanocomposites, J. Polym. Res. 20 (2013) 92, http://dx.doi.org/10.1007/s10965-013-0092-x.
[16] B.D. Malpass, Introduction to Industrial Polyethylene, John Wiley & Sons and Scrivener Publishing LCC, Salem, 2010.
[17] R. Jeziórska, B. Świerz-Motysia, M. Zielecka, A. Szadkowska, M. Studziński, Structure and mechanical properties of low-density polyethylene/spherical silica nanocomposites prepared by melt mixing: the joint action of silica's size, functionality, and compatibilizer, J. Appl. Polym. Sci. 125 (2012) 4326–4337, http://dx.doi.org/10.1002/app.36579.
[18] T. McNally, P. Pötschke, P. Halley, M. Murphy, D. Martin, S.E.J. Bell, G.P. Brennan, D. Bein, P. Lemoine, J.P. Quinn, Polyethylene multiwalled carbon nanotube composites, Polym. Guildf. 46 (2005) 8222–8232, http://dx.doi.org/10.1016/j.polymer.2005.06.094.
[19] T.-L. Wang, C.-C. Ou, C.-H. Yang, Synthesis and properties of organic/inorganic hybrid nanoparticles prepared using atom transfer radical polymerization,

J. Appl. Polym. Sci. 109 (2008) 3421–3430, http://dx.doi.org/10.1002/app.28462.
[20] V. Monteil, J. Stumbaum, R. Thomann, S. Mecking, Silica/Polyethylene nanocomposite particles from catalytic emulsion polymerization, Macromolecules 39 (2006) 2056–2062, http://dx.doi.org/10.1021/ma052737k.
[21] J. Zhu, S. Wei, Y. Li, L. Sun, N. Haldolaarachchige, D.P. Young, C. Southworth, A. Khasanov, Z. Luo, Z. Guo, Surfactant-free synthesized magnetic polypropylene nanocomposites: rheological, electrical, magnetic, and thermal properties, Macromolecules 44 (2011) 4382–4391, http://dx.doi.org/10.1021/ma102684f.
[22] A. Rungta, B. Natarajan, T. Neely, D. Dukes, L.S. Schadler, B.C. Benicewicz, Grafting bimodal polymer brushes on nanoparticles using controlled radical polymerization, Macromolecules 45 (2012) 9303–9311, http://dx.doi.org/10.1021/ma3018876.
[23] P.G. Ferreira, A. Ajdari, L. Leibler, Scaling law for entropic effects at interfaces between grafted layers and polymer melts, Macromolecules 31 (1998) 3994–4003, http://dx.doi.org/10.1021/ma9712460.
[24] C. Li, B.C. Benicewicz, Synthesis of well-defined polymer brushes grafted onto silica nanoparticles via surface reversible addition - fragmentation chain transfer polymerization, Macromolecules 38 (2005) 5929–5936, http://dx.doi.org/10.1021/ma050216r.
[25] O. Prucker, J. Rühe, Synthesis of poly(styrene) monolayers attached to high surface area silica gels through self-assembled monolayers of azo initiators, Macromolecules 31 (1998) 592–601, http://dx.doi.org/10.1021/ma970660x.
[26] C. Li, J. Han, C.Y. Ryu, B.C. Benicewicz, A versatile method to prepare RAFT agent anchored substrates and the preparation of PMMA grafted nanoparticles, Macromolecules 39 (2006) 3175–3183, http://dx.doi.org/10.1021/ma051983t.
[27] F. Dutertre, P.-Y. Pennarun, O. Colombani, E. Nicol, Straightforward synthesis of poly(lauryl acrylate)-b-poly(stearyl acrylate) diblock copolymers by ATRP, Eur. Polym. J. 47 (2011) 343–351, http://dx.doi.org/10.1016/j.eurpolymj.2010.12.003.
[28] Y. Li, B.C. Benicewicz, Functionalization of silica nanoparticles via the combination of surface-initiated RAFT polymerization and click reactions, Macromolecules 41 (2008) 7986–7992, http://dx.doi.org/10.1021/ma801551z.
[29] J. Gao, J. Li, B.C. Benicewicz, S. Zhao, H. Hillborg, L.S. Schadler, The mechanical properties of epoxy composites filled with rubbery copolymer grafted SiO2, Polym. (Basel) 4 (2012) 187–210, http://dx.doi.org/10.3390/polym4010187.
[30] M. Demetriou, T. Krasia-Christoforou, Synthesis and characterization of well-defined block and statistical copolymers based on lauryl methacrylate and 2-(acetoacetoxy)ethyl methacrylate using RAFT-controlled radical polymerization, J. Polym. Sci. Part A Polym. Chem. 46 (2008) 5442–5451, http://dx.doi.org/10.1002/pola.22863.
[31] C. Cobo Sánchez, M. Wåhlander, N. Taylor, L. Fogelström, E. Malmström, Novel nanocomposites of poly(lauryl methacrylate)-grafted Al2O3 nanoparticles in LDPE, ACS Appl. Mater. Interfaces 7 (2015) 25669–25678, http://dx.doi.org/10.1021/acsami.5b06427.
[32] A.K. Mallik, M.M. Rahman, M. Czaun, M. Takafuji, H. Ihara, Facile synthesis of high-density poly(octadecyl acrylate)-grafted silica for reversed-phase high-performance liquid chromatography by surface-initiated atom transfer radical polymerization, J. Chromatogr. A 1187 (2008) 119–127, http://dx.doi.org/10.1016/j.chroma.2008.02.011.
[33] M. Irani, H. Ismail, Z. Ahmad, Preparation and properties of linear low-density polyethylene-g-poly (acrylic acid)/organo-montmorillonite superabsorbent hydrogel composites, Polym. Test. 32 (2013) 502–512, http://dx.doi.org/10.1016/j.polymertesting.2013.01.001.
[34] J. Khan, S.E. Harton, P. Akcora, B.C. Benicewicz, S.K. Kumar, Polymer crystallization in nanocomposites: spatial reorganization of nanoparticles, Macromolecules 42 (2009) 5741–5744, http://dx.doi.org/10.1021/ma900794t.
[35] E. Roumeli, E. Pavlidou, A. Avgeropoulos, G. Vourlias, D.N. Bikiaris, K. Chrissafis, Factors controlling the enhanced mechanical and thermal properties of nanodiamond-reinforced cross-linked high density polyethylene, J. Phys. Chem. B 118 (2014) 11341–11352, http://dx.doi.org/10.1021/jp504531f.
[36] C.Y. Chee, N.L. Song, L.C. Abdullah, T.S.Y. Choong, A. Ibrahim, T.R. Chantara, C.Y. Chee, N.L. Song, L.C. Abdullah, T.S.Y. Choong, A. Ibrahim, T.R. Chantara, Characterization of mechanical properties: low-density polyethylene nanocomposite using nanoalumina particle as filler, J. Nanomater 2012 (2012) 1–6, http://dx.doi.org/10.1155/2012/215978.